CHEMISTRY
A EUROPEAN JOURNAL

DOI: 10.1002/chem.200700576

Environmental Factors Differently Affect Human and Rat IAPP: Conformational Preferences and Membrane Interactions of IAPP17–29 Peptide Derivatives**

Giuseppe Pappalardo,[a] Danilo Milardi,[a] Antonio Magrì,[a] Francesco Attanasio,[a] Giuseppe Impellizzeri,[b] Carmelo La Rosa,[b] Domenico Grasso,[b] and Enrico Rizzarelli*[b]

Abstract: Interest in the 37-residue human islet amyloid polypeptide (hIAPP) is related to its ability to form amyloid deposits in patients affected by type II diabetes. Attempts to unravel the molecular features of this disease have indicated several regions of this polypeptide to be responsible for either the ability to form insoluble fibrils or the abnormal interaction with membranes. To extend these studies to peptides that enclose His18, whose ionization state is believed to play a key role in the aggregation of hIAPP, we report on the synthesis of two peptides, hIAPP17–29 and rIAPP17–29, encompassing the 17–29 sequences of human and rat IAPP, respectively, as well as on their conformational features in water and in several membrane-mimicking environments as revealed by circular dichroism (CD) and 2D-NMR studies. hIAPP17–29 adopts a β-sheet structure in water and its solubility increases at low pH. Anionic sodium dodecyl sulfate (SDS) micelles promoted the formation of an α-helical structure in the peptide chain, which was poorly influenced by pH variations. rIAPP17–29 was soluble and unstructured in all the environments investigated, with a negligible effect of pH. The membrane interactions of hIAPP17–29 and rIAPP17–29 were assessed by recording differential scanning calorimetry (DSC) measurements aimed at elucidating the peptide-induced changes in the thermotropic behaviour of zwitterionic (DPPC) and negatively charged (DPPC/DPPS 3:1) model membranes (DPPC = 1,2-dipalmitoyl-*sn*-glycero-3-phosphocholine, DPPS = 1,2-dipalmitoyl-*sn*-glycero-3-phosphoserine). Results of DSC experiments demonstrated the high potential of hIAPP17–29 to interact with DPPC membranes. hIAPP17–29 exhibited a negligible affinity for negatively charged DPPC/DPPS model membranes at neutral pH. On the other hand, rIAPP17–29 did not interact with neutral or negatively charged membranes. The role played by His18 in the modulation of the biophysical properties of this hIAPP region was assessed by synthesising and studying the R18HrIAPP17–29 peptide; the replacement of a single Arg with a His residue is not sufficient to induce either amyloidogenic propensity or membrane interaction in this region. The results show that the 17–29 domain of hIAPP has many properties of the full-length protein "in vitro" and this opens up new perspectives for both research and eventually therapy.

Keywords: amylin · circular dichroism · IAPP · membranes · peptides

Introduction

Numerous neurodegenerative and systemic diseases have been associated with aggregating proteins or peptides.[1–3] These protein aggregates, known as amyloids, have shown significant toxicity "in vitro" and "in vivo".[4–7] The formation of amyloid structures can be generated both from globular proteins that self assemble to form aggregates starting from a folded state[8] and from proteins or polypeptides that lack a well-defined globular structure in their unaggregated state.[9] Typical examples of this second group include Aβ amyloid,[10,11] the proteolytic fragment that forms amyloid

[a] Dr. G. Pappalardo, Dr. D. Milardi, Dr. A. Magrì, Dr. F. Attanasio
Istituto di Biostrutture e Bioimmagini
Consiglio Nazionale delle Ricerche Viale A. Doria 6
95125 Catania (Italy)

[b] Prof. G. Impellizzeri, Dr. C. La Rosa, Prof. D. Grasso, Prof. E. Rizzarelli
Dipartimento di Scienze Chimiche
Università degli Studi di Catania Viale A. Doria 6
95125 Catania (Italy)
Fax: (+39) 095-337-678
E-mail: erizzarelli@dipchi.unict.it

[**] IAPP = islet amyloid polypeptide

Supporting information for this article is available on the WWW under http://www.chemeurj.org/ or from the author.

deposits in Alzheimer's disease, and Amylin, also known as islet amyloid polypeptide (IAPP). The IAPP polypeptide is involved in the regulation of carbohydrate metabolism[12] and is responsible for amyloid formation in type II diabetes.[13–16] IAPP is composed of 37 amino-acid residues, containing a disulfide bridge between residues 2 and 7 and an amidated C terminus. Although in humans and a few other mammals such as primates[17] and cats[18] it might form amyloid deposits, associated with areas of pancreatic β-cell dysfunction, in rats it does not form amyloid fibrils and it is not cytotoxic.[19,20] The human (hIAPP) and rat (rIAPP) sequences differ in only six out of 37 positions, five of which are located between residues 20–29. rIAPP contains three proline residues in this region at positions 25, 28 and 29, whereas the human sequence has none (Scheme 1). Additional differences include the replacement of His18, Phe23 and Ile26 of the human sequence with Arg, Leu and Val, respectively, in rIAPP.

Scheme 1. Primary sequences of human and rat amylin peptides. The six residues that are different in human and rat amylin are indicated in boxes.

Amyloidogenic hIAPP has been shown to be more toxic to cells than non-amyloidogenic rat IAPP.[21] To explain this different behaviour from a primary-structure perspective, attention was focused initially on the region encompassing residues 20–29. Some authors attributed to this region a key role in amyloid formation and showed that a peptide fragment corresponding to residues 20–29 of hIAPP was capable of forming amyloids "in vitro".[22] A large number of variants of the 20–29 fragment, including a systematic set of proline-substituted ones, were investigated to identify the key residues for amyloid formation in this system.[23–25] Other domains of IAPP have been studied and peptides encompassing residues 8–20, 10–19, 20–29, 30–37 and 8–37 of hIAPP have been found to form amyloids.[26–29] Although the 20–29 segment is not the only amyloidogenic region of hIAPP, it has been widely used as a model system for biophysical studies of amyloid formation.[29,30] Smaller peptides derived from this domain also form amyloid; the peptide containing the residues 22–27 (Asn-Phe-Gly-Ala-Ile-Leu or NFGAIL) has been proposed as the minimal amyloid-forming sequence of hIAPP.[29] More recently, it has been reported that although the three proline residues play a dominant negative role in fibril formation, their presence is not sufficient to completely prevent rIAPP forming fibrils, because each one of the other three residues (i.e, Arg18, Leu23 and Val26) also has a non-negligible effect in promoting IAPP aggregation.[31] Peptides derived from the 10–20 region of hIAPP have been shown to accelerate fibrillogenesis of full-length IAPP, supporting the conclusion that amyloidogenic properties of hIAPP cannot be simply ascribed to the sequence of the 20–29 region.[32,33] The observation that His18 protonation might modulate aggregation of full-length hIAPP is noteworthy[33] and is consistent with a recently described model of hIAPP fibrils,[34] in which individual peptides form a planar S-shaped structure, involving residues 9–37, that is characterised by the presence of three β strands with His18 located in the turn between strands 1 and 2. The supposedly parallel in-register stacking of these basic building blocks would bring His18 close in space in neighbouring peptides. Such a structure would likely be strongly destabilised by electrostatic repulsion upon protonation of His18. However, it should be noted that the effect of histidine as a major trigger of fibril formation was not confirmed by another study in which hIAPP fibrillogenesis was found to be independent of pH within the physiological range.[35] In addition, several studies suggest that the mechanism triggering amyloid disease appears to be linked to an abnormal interaction between amyloidogenic proteins and lipid membranes.[36–38] The mode of interaction of such proteins and/or their peptide fragments with membranes has not yet been elucidated, although several hypotheses have been suggested: membranes have been implicated both as the targets of toxicity, through membrane destabilization, as well as the catalysts that facilitate protein aggregation.[39–44] More recently, a common structural factor involved in protein-misfolding diseases has been proposed, based on the evidence that various amyloid molecules form porelike structures and elicit harmful ion-channel activity in cell membranes.[45] This hypothesis provides a molecular mechanism for amyloid pathogenesis that is consistent with recent observations that the polymerization of amyloid peptides is a stepwise process, with early events leading to the formation of small oligomers, followed by assembly into soluble protofibrils and then insoluble fibrils.[46] IAPP forms voltage-dependent ion-selective pores in planar lipid bilayers,[47] to mediate vesicle aggregation and to induce leakage of lipid-vesicle contents through a "porelike" mechanism.[48–50] Finally, recent reports show that membranes containing negatively charged lipids accelerate the kinetics of IAPP fibrillization.[51,52] However, despite the growing body of evidence implicating membrane interaction in IAPP toxicity, the molecular aspects of the interaction with lipid membranes have not yet been characterised in detail.

To shed light on the role played by His18, Pro28 and Pro29 in modulating the structure and membrane activity of IAPP, we investigated the conformation and the ability to perturb model membranes of three newly synthesised peptides encompassing residues 17–29 of the human IAPP (hIAPP17–29), its rat analogue (rIAPP17–29) as well as a rat derivative in which the Arg18 is replaced by a His (R18HrIAPP17–29). Circular dichroism (CD) and NMR experiments were carried out to study the effect of different factors such as pH or different membrane-mimicking environments on their conformational properties. Moreover, differential scanning calorimetry (DSC) experiments were performed to see if the synthesised peptides were able to modify the thermotropic behaviour of zwitterionic (DPPC) or negatively charged (DPPC/DPPS 3:1) model membranes

(DPPC = 1,2-dipalmitoyl-*sn*-glycero-3-phosphocholine, DPPS = 1,2-dipalmitoyl-*sn*-glycero-3-phosphoserine). The analysis of the DSC profiles of lipid/peptide systems were validated by control experiments carried out in parallel on the full-length proteins hIAPP and rIAPP and helped to clarify not only the effects of the peptide on the physical state of the membrane, but also the topological arrangement of the peptide inserted into the lipid matrix. Furthermore, DSC analysis of DPPC/hIAPP17–29 and DPPC/R18HrIAPP17–29 systems titrated with increasing amounts of copper(II) ions, allowed us to establish whether the His18 residue binds copper(II) and, consequently, affects the lipid/peptide interaction. This novel use of the His residue as a copper(II)-sensitive "built-in probe" was helpful in assessing the arrangement of the IAPP fragments with respect to the host membrane.

Results

Structural characterization of the 17–29 IAPP domains in different environments

Effect of pH on the conformation of hIAPP17–29, rIAPP17–29 and R18HrIAPP17–29 in aqueous solutions: Due to the poor solubility of hIAPP17–29 in water, clear solutions of this peptide were obtained only at a concentration of 10^{-5} mol dm^{-3}. The far-UV CD spectra of the homogeneous solutions recorded at different pH values display intense positive bands within the 200–210 nm region along with negative ellipticity at 220–230 nm (Figure 1a). A neat decrease in the negative-band intensity was observed as the pH value increased from 6.5 to 7.5; this pH interval indicates that charge neutralisation of the imidazole side chain may be mainly responsible for this effect. Such an effect was accompanied by macroscopic changes in the sample solution, which became turbid. The shape of the CD curves is of the class B type and is typical of β-sheet or β-turn conformations.[53] Furthermore, the lack of homogeneity between the obtained spectral profiles provides evidence for the remarkable tendency of hIAPP17–29 to aggregate. By contrast, CD spectra obtained for rIAPP17–29 under the same experimental conditions invariably showed negative ellipticity below 200 nm regardless of the pH of the solution (Figure 1b), thus suggesting a random-coil structure.[54] R18HrIAPP17–29 showed a conformational behaviour similar to rIAPP17–29 (CD spectra not shown). This finding supports the hypothesis that the Pro residues of the rat sequence play a major role in preventing the self-assembly and the consequent precipitation of the peptide.

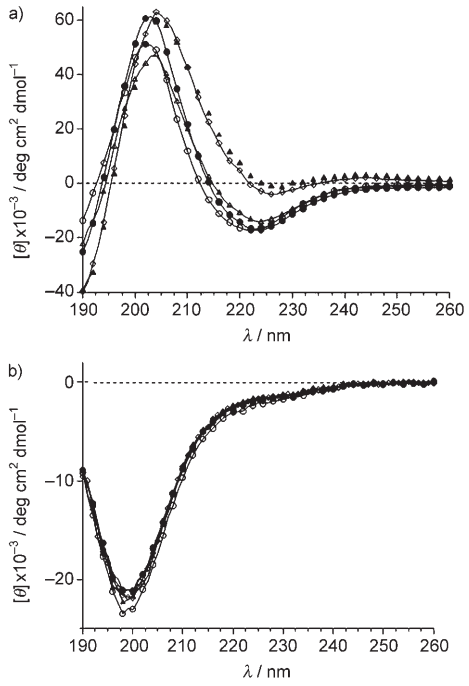

Figure 1. CD spectra of a) hIAPP17–29 and b) rIAPP17–29 recorded in H_2O at different pH values (pH 5 = ○; pH 6 = ●; pH 7 = △; pH 8 = ▲; pH 9 = ◇).

HIAPP17–29 undergoes conformational transition in the presence of trifluoroethanol (TFE): In a 50% TFE/water mixture, the solubility of hIAPP17–29 moderately increases and this makes it possible to obtain CD spectra at concentrations equal to 1×10^{-4} mol dm^{-3}. Under these experimental conditions the obtained CD spectra were characterised by two negative signals at 204 and 220 nm and a positive band at 193 nm, indicating the presence of α-helical conformation. Notably, the negative band at 204 nm is wider than that at 220 nm; this, together with the crossover wavelength value (λ_0) observed at around 196 nm, suggests that the peptide can adopt only a partial α-helical structure. In fact, in the CD spectrum of hIAPP17–29 recorded in 100% TFE, the two negative peaks have roughly the same intensity and the λ_0 value shifts to approximately 200 nm, as typically observed for fully α-helical peptides (Figure 2a).[54] Differently from hIAPP17–29, the CD spectra of rIAPP17–29 in TFE do not change, and are characteristic of a random-coil conformation (Figure 2b). Figure 2 also shows that pH changes have negligible effects on the conformation of both peptides.

Conformational features of hIAPP17–29 and rIAPP17–29 in the presence of SDS micelles: To investigate the conformational features of hIAPP17–29 in a membrane-mimicking environment, CD spectra were also recorded in the presence of sodium dodecyl sulfate (SDS). SDS has been extensively used for structural investigations of membrane peptides as it provides a hydrophobic environment that mimics either biological membranes or the interior of proteins.[55] Based on the above, we recorded a series of CD spectra at different SDS concentrations (below and above the critical micelle concentration, CMC) to investigate any conformational polymorphism that might occur in hIAPP17–29. The CD measurements carried out in the presence of SDS (1×10^{-5} mol dm^{-3}) at different pH values invariably indicate the presence of a β-sheet peptide conformation (see Figure 3a).

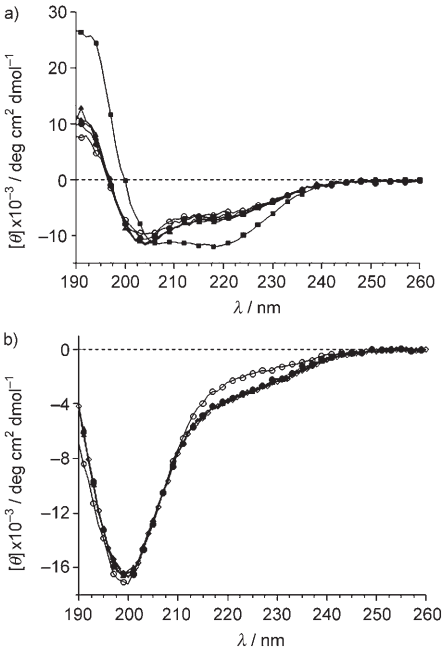

Figure 2. CD spectra of a) hIAPP17–29 and b) rIAPP17–29 recorded in 50% TFE at different pH values. (pH 5 = ○; pH 6 = ●; pH 7 = △; pH 8 = ▲; pH 9 = ◇; 100% TFE = ■).

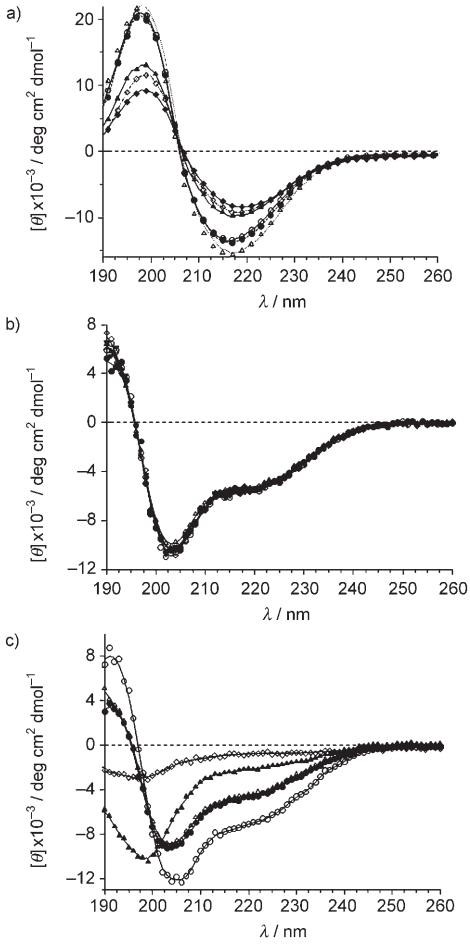

Figure 3. CD spectra of hIAPP17–29 collected at different pH values in the presence of a) 1×10^{-5} mol dm^{-3} (pH 5 = ○; pH 5.5 = ●; pH 6 = △; pH 6.5 = ▲; pH 7.5 = ◇; pH 8.5 = ◆) and b) 1.7×10^{-1} mol dm^{-3} of SDS (pH 5 = ○; pH 6 = ●; pH 7 = △; pH 8: ▲; pH 9 = ◇). c) CD spectra of hIAPP17–29 recorded at pH 7.4 at different concentrations of SDS (panel c, 1.7×10^{-1} mol dm^{-3}: ○; 3.4×10^{-2} mol dm^{-3}: ●; 1.7×10^{-2} mol dm^{-3}: △; 3.4×10^{-3} mol dm^{-3}: ▲; 1.7×10^{-3} mol dm^{-3}: ◇).

The spectral amplitude decreases as pH increases. In particular, no precipitate was detected over the pH range 4.7–6.1; CD curves are unaffected by the pH increase. On the contrary, precipitation was detectable with the naked eye over the pH range 6.5–8.5; CD curves collected within this pH range show a decreased intensity. Spectral amplitude changes at around pH 6.0, which is close to the p*K* value of the imidazole residue of histidine; likely the neutralisation of the histidine side chain may accelerate the aggregation process of hIAPP17–29. On the other hand, CD spectra recorded in the presence of SDS micelles (1.7×10^{-1} mol dm^{-3}) show two minima at 204 nm and 220 nm and a positive ellipticity at 190 nm, which is consistent with a partial α-helical structure in solution. In this latter case, however, both the intensity and shape of the CD curves do not seem to be affected by the pH change (Figure 3b). Unexpectedly, CD experiments, performed by adding the same amount of hIAPP17–29 dissolved in aqueous SDS (1.7×10^{-1} mol dm^{-3}) to a series of increasingly diluted SDS solutions, result in spectral changes that are consistent with the conversion from a predominant α-helical conformation to unstructured peptide chains at SDS concentrations above and below the CMC, respectively (Figure 3c).

This is likely due to the presence of preformed aggregates in aqueous SDS solutions of 1×10^{-5} mol dm^{-3}.[33] 1.7×10^{-1} mol dm^{-3} SDS is expected to disaggregate the peptide chains and cause the peptide to assume a helical structure. Upon SDS dilution, the α-helix-stabilising effect, generated by the hydrophobic micellar environment, becomes increasingly weaker, thus causing the peptide chains to become unstructured and to interact with one another. Perhaps the structures observed at low SDS concentrations might represent the seed that preludes the subsequent aggregation process. The observation of a decreased amplitude of the spectrum recorded at 1.7×10^{-3} mol dm^{-3} SDS supports this hypothesis. Again, analogous CD experiments carried out on the rIAPP17–29 show that neither 3.4×10^{-2} mol dm^{-3} nor 1.7×10^{-1} mol dm^{-3} SDS solutions were able to perturb the CD profiles, which remained typical of an unstructured peptide backbone (Figure 4a and b).

Electrostatic interactions are important determinants for the hIAPP17–29 conformational polymorphism: The presence of an α-helix structure in TFE or SDS micelles is in keeping with a hydrophobic environment assisting both dissolution and secondary-structure formation of the peptide chain. Unlike TFE, however, SDS micelles have a neat negative charge on their surface, indicating that the electrostatic effect plays a role in the induction of α-helical structure. To verify this hypothesis, CD experiments were carried out in

the presence of uncharged micelles made up of a neutral detergent (dodecyl-β-maltoside, DβM). None of the conformational changes observed in SDS are detected in DβM. The CD curves (Figure 5a) rather recall those observed in water; in addition, the solution turns turbid at around pH 7, thus supporting the hypothesis of the presence of pre-assembled β-sheet-rich peptides. The effect of charged micelles in assisting the conformational transition toward the α helix was demonstrated by titrating a pH-4 solution of hIAPP17–29 in 1.7×10^{-1} mol dm^{-3} of DβM, with increasing amounts of an equimolar SDS solution with the same pH value. The CD curves shown in Figure 5b clearly indicate a β-sheet/α-helix conformational transition resulting from the increasing SDS concentration. Interestingly, once hIAPP17–29 interacts with SDS micelles it cannot be taken back to its original β-sheet conformation (not shown).

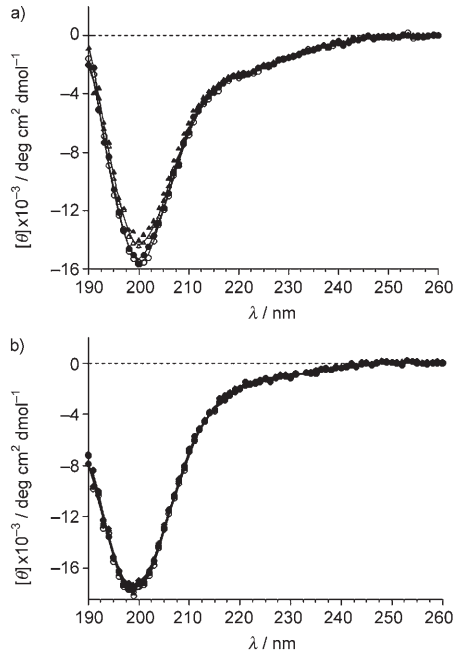

Figure 4. CD spectra of rIAPP17–29 recorded in a) 3.4×10^{-2} mol dm^{-3} SDS or b) 1.7×10^{-1} mol dm^{-3} SDS at different pH values. (pH 5 = ○; pH 6 = ●; pH 7 = △; pH 8 = ▲; pH 9 = ◇).

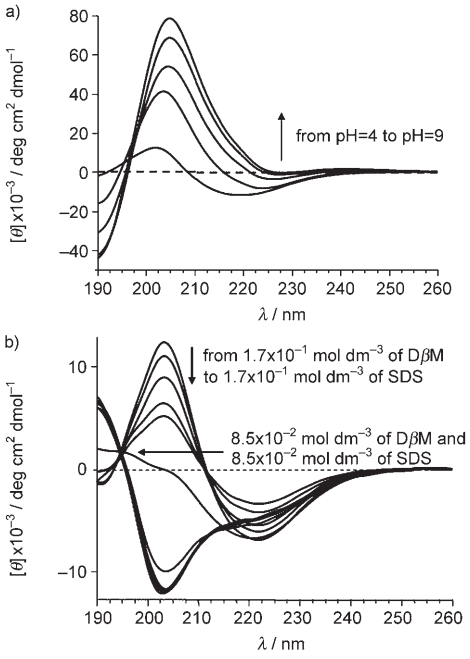

Figure 5. a) CD spectra of hIAPP17–29 recorded in aqueous DβM (1.7×10^{-1} mol dm^{-3}) at different pH values. b) CD curves recorded at pH 4 by titrating an aqueous solution of hIAPP17–29 in 1.7×10^{-1} mol dm^{-3} DβM with increasing aliquots of a SDS solution of 1.7×10^{-1} mol dm^{-3}.

Fibril formation: The thioflavine-T binding assay was used to see whether or not ordered β-sheet aggregates were present in the aqueous solutions studied (Figure 6). rIAPP17–29 did not reveal the presence of amyloid structures at the two pH values studied, as expected. The human peptide sequence shows a dependence on the pH that induces a slight fluorescence enhancement of thioflavine-T at pH 4 over the time monitored. Conversely, the peptide solution at pH 7.4 shows a sharp increase of thioflavine-T fluorescence, indicating the presence of amyloid-like structures.

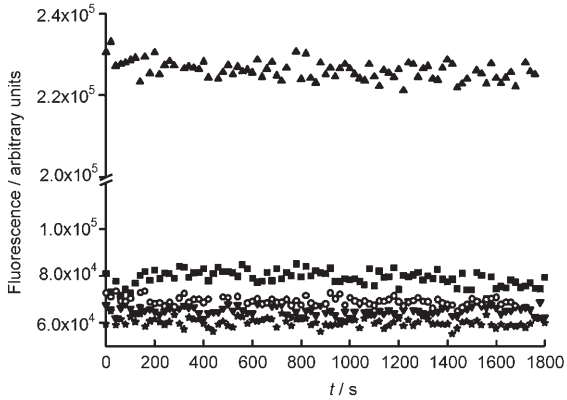

Figure 6. ThT fluorescence profiles of rIAPP17–29 and hIAPP17–29 samples monitored at different pH values. THT: ⋆; hIAPP17—29 at pH 4: ■; hIAPP17—29 at pH 7.4: ▲; rIAPP17—29 at pH 4: ▼; rIAPP17—29 at pH 7.4: ○.

NMR of hIAPP17–29 in SDS micelles: The solubility of hIAPP17–29 in water was too low to permit a detailed NMR study. However, NMR spectra could be collected in the presence of SDS micelles, (^{1}H resonance assignments are reported in the Supporting Information Table 1S). NMR experiments were carried out with one millimolar sample at pH 4.5. The COSY and TOCSY spectra facilitated the assignment of individual spin systems, whereas the sequence-specific assignments were accomplished through analysis of the NOE connectivities observed in the NOESY experiments.[56–58] The presence of secondary structures was verified by examining the NOESY spectra for distinctive sequential and medium-range NOEs in addition to the analysis of C_αH secondary chemical shifts relative to random-coil

values ($\Delta\delta C_\alpha H = \delta C_\alpha H_{observed} - \delta C_\alpha H_{random\ coil}$).[59,60] Although the observation of a number of sequential $d_{NN(i,i+1)}$ connectivities implies that the peptide can adopt an α-helical structure, the presence of $d_{\alpha N(i,i+1)}$ and $d_{\beta N(i,i+1)}$ contacts supports the presence of extended peptide chains (Figure 7a and b).

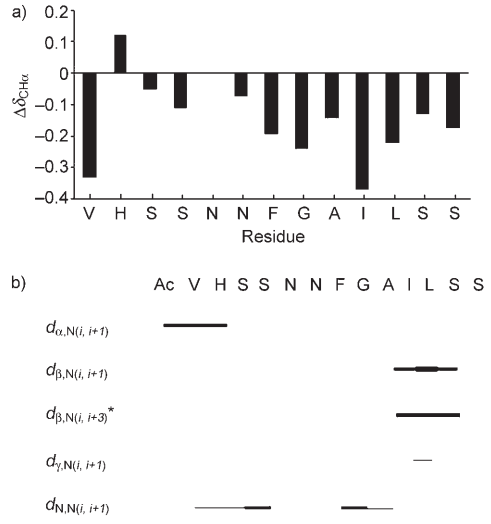

Figure 7. Chemical shifts and NOE connectivities of hIAPP17–29 in SDS micelles. a) Comparison of $C_\alpha H$ chemical-shift deviations from random-coil values of residues ($\Delta\delta_{C\alpha H}$) measured in 1.7×10^{-1} mol dm^{-3} SDS at 27 °C and pH 4.5; the random-coil values were recorded elsewhere.[60] b) Sequential and medium-range NOE connectivities observed in 1.7×10^{-1} mol dm^{-3} SDS at 27 °C and pH 4.5. The thickness of the lines reflects the relative intensities of the NOE signals. *Could be also assigned to an intra-residue $d_{\alpha N}$ of the Ala25.

However, the majority of the $\Delta\delta C_\alpha H$ are negative and this is compatible with the tendency of the peptide chain to fold into an α-helical conformation. On the other hand, additional inter-residue NOE contacts are detected and specifically assigned as follows: ^{26}Ileβ–^{19}SerNH, Benzyl-(2,6)^{23}Phe–^{26}IleγCH_3 (or ^{27}LeuδCH_3), ^{5}Asnα–^{26}IleγCH_2, ^{18}Hisβ–^{26}IleγCH_2. These unusual NOEs reflect a close proximity of the involved side chains and may result from conformational flexibility of the peptide main chain or, more significantly, from the interaction between different peptide chains. As indicated by CD spectra, rIAPP17–29 does not tend to undergo a random coil→α-helix transition. To better check this aspect, NMR experiments were run in 9:1 H_2O/D_2O. The structural information derived from the NMR experiments is consistent with CD results: the extent of the $C_\alpha H$ chemical shifts was predictably not significant due to conformational averaging.[59] Moreover, the 2D NMR spectra do not show any inter-residue interactions that might indicate a preferred secondary structure. Instead, the observation of sequential $d_{\alpha N}$ or $d_{\beta N}$ NOE connectivities only together with intra-residue dipolar contacts are consistent with an unstructured and flexible peptide backbone (see Supporting Information Table 2S and Figures 1S and 2S).

Membrane perturbation induced by IAPP and related peptide fragments

DSC of DPPC/hIAPP1–37 and DPPC/rIAPP1—37: The DSC curves of DPPC/rIAPP (curve a) and DPPC/hIAPP (curve b) prepared according to method A (see Experimental Section) are reported in Figure 8 and compared with the

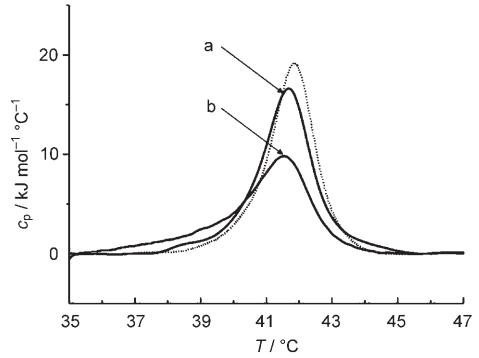

Figure 8. Heat-capacity profiles (c_p) of MLVs of a) DPPC/rIAPP1–37 and b) DPPC/hIAPP1–37, obtained by preparing the lipid/peptide systems according to method A reported in the Experimental Section. The DSC profile of the pure DPPC (dotted line) is also reported for comparison.

DSC curve of pure DPPC multilamellar vesicles (MLV) (dotted line). These results show that the thermally induced transition of DPPC membranes is differently affected by the presence of human and rat IAPP. In particular, when human IAPP is inserted into the membrane, the DSC peak corresponding to the thermally induced main transition of the membrane broadens and shifts to lower temperatures (transition temperature $T_m = 41.5$ °C) relative to the case with pure DPPC. Moreover, the transition enthalpy decreases from 36.0 to 28.2 kJ mol^{-1}. The perturbation of the membrane induced by the rat derivative is less severe: T_m is shifted to 41.7 °C and ΔH decreases from 36.0 to 35.8 kJ mol^{-1}.

Though DSC as a tool to investigate the peptide-induced perturbation of lipid bilayers was described elsewhere,[61] we would like to recall that heat-capacity (c_p) changes concerning the main transition of lipid/peptide systems may help to clarify not only the effects of the presence of the peptide on the physical state of the membrane, but also the topological arrangement of the peptide inserted into a lipid matrix. In fact, the enthalpy change observed during the lipid main transition is mainly ascribable to the packing efficiency of the hydrocarbon tails.[62] The peptide-induced decrease of the transition enthalpy of the bilayer may thus be related to the extent of the interaction between guest molecules and the core of lipid membranes. Moreover, T_m is more sensitive to interactions involving the lipid head groups, and increases when the membrane surface is involved in the interaction with the guest peptide.[63–65] Our results for full-length hIAPP and rIAPP are in agreement with previous literature data and support the potential of DSC as an effective tool in the investigation of IAPP-induced lipid membrane perturbation.[47]

In this context, the three IAPP derivatives encompassing residues 17–29 were incorporated into DPPC vesicles and studied by DSC.

Effects of incorporation of hIAPP17–29, rIAPP17–29 and R18HrIAPP17–29 peptides into DPPC vesicles: Figure 9 shows the DSC curves obtained for DPPC/hIAPP17–29 (curve a), DPPC/rIAPP17–29 (curve b) and DPPC/R18HrIAPP17–29 (curve c) prepared according to method A described in the Experimental Section. The thermally induced transition of DPPC is differently affected by the three peptides. In particular, when the hIAPP17–29 peptide is inserted into the membrane, the ΔH associated to the DSC peak decreases from 36 to 24 kJ mol^{-1}.

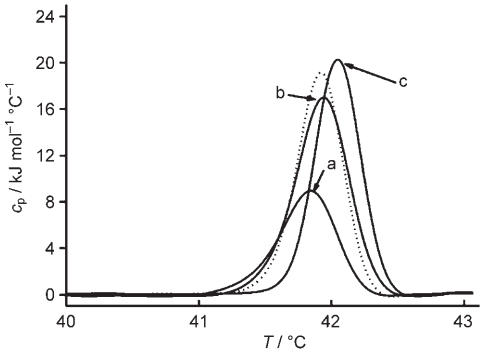

Figure 9. Heat-capacity profiles (c_p) of MLVs of a) DPPC/hIAPP17–29, b) DPPC/rIAPP17–29, and c) DPPC/R18HrIAPP17–29 obtained under the experimental conditions reported in the text. The DSC profile of the pure DPPC (dotted line) is also reported for comparison.

Moreover, the DSC analysis of DPPC/hIAPP17–29 systems having a peptide/lipid ratio of 1:20 shows a decrease in the transition enthalpy of the membrane proportional to the amount of peptide added (see Table 1).

Table 1. Calorimetric parameters [ΔH in kJ mol^{-1}] and temperatures [T_m in °C].[a]

System	Peptide/lipid ratio	ΔH	T_m
DPPC	–	36.4 (1.6)	41.9 (0.1)
DPPC/hIAPP	1:50	28.2 (1.5)	41.5 (0.1)
DPPC/rIAPP	1:50	35.8 (1.4)	41.7 (0.1)
DPPC/hIAPP17–29	1:20	24.3 (1.3)	41.8 (0.1)
DPPC/hIAPP17–29	1:10	26.1 (1.2)	41.8 (0.1)
DPPC/rIAPP17–29	1:10	35.4 (1.5)	41.9 (0.1)
DPPC/R18HrIAPP17–29	1:10	36.0 (1.6)	42.1 (0.1)

[a] Values relative to the main transition of different peptide/lipid bilayer systems prepared according to method A reported in the Experimental Section. Experimental values are reported as mean of three repeated experiments. Standard deviation is reported in parentheses.

This shows that the perturbation of the DPPC membrane induced by hIAPP17–29 depends on the concentration of the guest peptide. On the contrary, the close similarity of the DSC curves concerning the transitions of pure DPPC and DPPC/rIAPP17–29 indicates that this peptide does not interact with the membrane. DSC experiments were also carried out on DPPC/R18HrIAPP17–29 to shed light on the role played by His18 in the interaction with the membrane. The interaction of the R18HrIAPP17–29 peptide with the membrane is quite negligible and is associated with both a slight shift of T_m towards higher temperatures and a negligible change in the transition enthalpy. All the calorimetric parameters are listed in Table 1.

Effect of copper(II) on peptide/DPPC systems: His is known to be an anchoring site for copper(II) in proteins, due to the high affinity of the imidazole nitrogen for this metal ion. Moreover, His residues are not hydrophobic and thus, in membrane-active peptides, they usually do not interact with the hydrocarbon interior of the lipid bilayer. Instead, they are generally located on the hydrophilic surface of the membrane and may contribute to controlling the interaction of the peptide with the membrane. If His residues are exposed to the solvent, they might bind copper(II) ions and consequently modify their conformation and/or ability to interact with the membranes. Based on these considerations, the His18 residue may be considered as an effective "built-in probe" to monitor the position of IAPP fragments in model membranes.

The DPPC/peptide systems were titrated with copper(II); these DSC experiments provide information about the copper(II)-induced changes in the thermotropic behaviour of the lipid/peptide systems, and consequently, also about the position of His residues and the topology of the lipid/peptide system. The addition of copper(II) produces a remarkable effect (see Figure 10) only when R18HrIAPP17–29 is inserted in the membrane (prepared according to method A, peptide/copper(II) molar ratio 1:1, 1:2, 1:3, 1:4, 1:5, 1:6). In particular, at a copper(II) concentration of 3×10^{-5} mol dm^{-3} (i.e., peptide/copper(II) molar ratio 1:1) the DSC peak broadens and shifts towards lower temperatures.

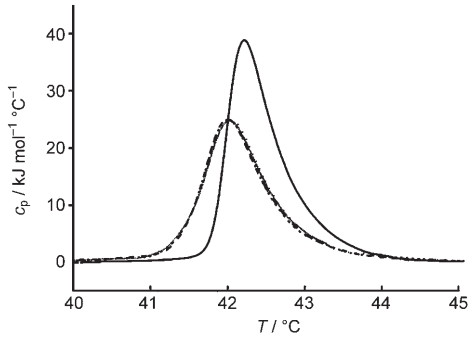

Figure 10. Heat-capacity profiles (c_p) of MLVs of 10:1 DPPC/R18HrIAPP17–29 (——), 10:1:1 DPPC/copper(II)/rIAPP17–29 (– – –), 10:2:1 DPPC/copper(II)/rIAPP17–29 (•••••). c_p profiles of 10:3:1, 10:4:1, 10:5:1 and 10:6:1 DPPC/copper(II)/R18HrIAPP17–29 systems obtained under the experimental conditions reported in the text were indistinguishable from the 10:1:1 and 10:2:1 systems and were not reported.

Moreover, the transition enthalpy decreases and this indicates a deeper penetration of the peptide into the hydrophobic region of the bilayer. All DSC curves have the same profile over the range of copper(II)/peptide molar ratios 1:2–1:6. Control experiments were carried out on pure DPPC large unilamellar vesicles (LUV)/copper(II) samples with increasing copper(II) concentrations: copper(II) addition did not produce any effect when added to DPPC/hIAPP17–29 systems regardless of the preparation method adopted. This indicates that R18HrIAPP17–29 is not deeply inserted into the membrane and its interaction with the membrane takes place mainly at the surface of the bilayer. As a consequence, the His18 residue is exposed to the solvent and can bind copper(II) with a 1:1 stoichiometry (see Figure 10), thus affecting the ability of these peptides to interact with DPPC vesicles and to modify their DSC response. On the contrary, the interaction of hIAPP17–29 with DPPC probably buries the His18 residue more deeply in the interior of the model membrane and prevents any interaction with copper(II) ions.

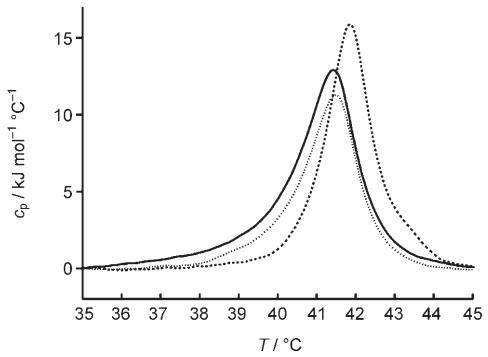

Figure 11. Heat-capacity profiles (c_p) of LUVs of pure DPPC (——), of the first (– – –) and second (•••••) heating of 10:1 DPPC/hIAPP17–29 systems obtained under the experimental conditions reported in the text. The DSC profiles of the third and fourth heating were indistinguishable from the second scan and were not reported.

Effects of addition of hIAPP17–29, rIAPP17–29 to the external surface of zwitterionic DPPC and negatively charged DPPC/DPPS vesicles: To fully describe the different abilities of the hIAPP17–29 and rIAPP17–29 to interact with model membranes, their interactions with the external side of the lipid bilayer needs to be investigated. Large unilamellar vesicles (LUVs) are the most suitable models for these investigations: they are stable, unilamellar, and have a high surface/weight ratio. To assess the potential of a peptide to interact with the membrane surface, the thermotropic behaviour of LUVs after incubation with the peptide may be conveniently studied. The potential of hIAPP17–29 to interact with the neutral surface of DPPC LUVs was investigated by analysing the DSC curves of the lipid/peptide systems prepared according to method B (see Experimental Section). The DSC curves of DPPC LUVs after incubation with hIAPP17–29 in a lipid/peptide ratio of 10:1 are reported in Figure 11.

The dashed curve reported in Figure 11 represents the DSC curve obtained after the first heating of the sample. These DSC curves are descriptive of the interaction of the peptide with the membrane in the gel state. In this case hIAPP17–29 induces an increase in the T_m and only a slight decrease in ΔH; this suggests an interaction occurring mainly at the surface of the membrane. After the first heating, the peptide interacts with the liquid-crystalline membrane, which is known to be more fluid. The second heating of the lipid/peptide sample (dotted line) evidences a decrease in both T_m and ΔH. This indicates that hIAPP17–29 may penetrate more deeply into the membrane when it is in a liquid-crystalline state. Notably, after four repeated heating-cooling cycles (see Table 2) the calorimetric parameters of the lipid/peptide sample reach equilibrium values comparable to those obtained for the lipid dispersions in which the peptide was incorporated into the membrane (see Table 1).

Table 2. Calorimetric parameters [ΔH in kJ mol^{-1}] and temperatures [T_m in °C].[a]

System	I heating		II heating		III heating		IV heating	
	T_m	ΔH	T_m	ΔH	T_m	ΔH	T_m	ΔH
DPPC	41.6	31.7	41.4	29.5	41.4	29.5	41.4	29.5
	(0.1)	(2.1)	(0.1)	(2.1)	(0.1)	(2.1)	(0.1)	(2.1)
DPPC/hIAPP17–29	41.8	27.3	41.5	24.2	41.5	24.9	41.5	24.9
	(0.1)	(2.1)	(0.1)	(2.0)	(0.1)	(2.0)	(0.1)	(2.0)
DPPC/rIAPP17–29	41.7	29.6	41.4	28.0	41.4	27.0	41.4	26.4
	(0.1)	(2.2)	(0.1)	(2.2)	(0.1)	(2.2)	(0.1)	(2.2)
DPPC/DPPS 3:1	42.8	25.4	42.5	29.2	42.4	28.8	42.5	27.9
	(0.1)	(2.1)	(0.1)	(2.0)	(0.1)	(1.8)	(0.1)	(1.9)
DPPC/DPPS/hIAPP17–29	42.5	26.2	42.4	23.4	42.4	24.9	42.4	23.8
	(0.1)	(2.0)	(0.1)	(2.1)	(0.1)	(2.1)	(0.1)	(2.1)
DPPC/DPPS/rIAPP17–29	42.6	27.1	42.5	24.0	42.5	25.0	42.5	24.0
	(0.1)	(2.2)	(0.1)	(2.1)	(0.1)	(2.1)	(0.1)	(2.1)

[a] Values relative to the main transition of different peptide/lipid bilayer systems prepared according to method B reported in the Experimental Section. Membranes were always prepared as LUVs. The calorimetric parameters relative to repeated heating cycles (I–IV) are reported. Experimental values are reported as mean of three repeated experiments. Standard deviation is reported in parentheses.

The calorimetric parameters for LUVs of DPPC after incubation with rIAPP17–29 are also reported in Table 2. These data show that this fragment is not able to interact with the external surface of the DPPC membrane. DPPC/DPPS 3:1 LUVs were also prepared and incubated with hIAPP17–29 and rIAPP17–29, to investigate the potential role of electrostatic effects in enhancing the affinity of hIAPP17–29 for membranes. To ensure the complete mixing of DPPC and DPPS, several heating/cooling cycles of the membranes were carried out until a complete equilibrium

was reached and the DSC curves, as well as their relative calorimetric parameters, remained unchanged after repeated cycles (Table 2); the 3:1 DPPC/DPPS LUVs, that did not change after four heating/cooling cycles, were incubated with hIAPP17–29 or with rIAPP17–29 (Table 2). In this case, the two peptides exhibit an almost negligible interaction with the membrane. We also carried out a series of CD experiments in the presence of DPPC (Figure 12a) or, alternatively, 3:1 DPPS:DPPC small unilamellar vesicles (SUVs) (Figure 12b) to establish which conformer of hIAPP17–29 interacts with the lipid bilayer. Results typical of β-sheet conformations were obtained in both cases supporting the hypothesis that only pre-assembled β-sheet oligomers can interact with lipid bilayers. The physical state of the membrane (gel or liquid crystal) is not crucial for the conformational features of hIAPP17—29, as evidenced by the similarity of hIAPP17–29/DPPC and hIAPP17–29/DPPC/DPPS CD curves obtained at temperatures below and above the main transition of the lipid bilayer (Figure 12). However, it should be pointed out that only in the case of DPPC may the peptide interact with the membrane. On the contrary, in the presence of 30% of DPPS the peptide does not interact with the membrane and rapidly precipitates, probably owing to the higher rigidity of the lipid matrix and to the higher aggregation kinetics promoted by the negative charges.

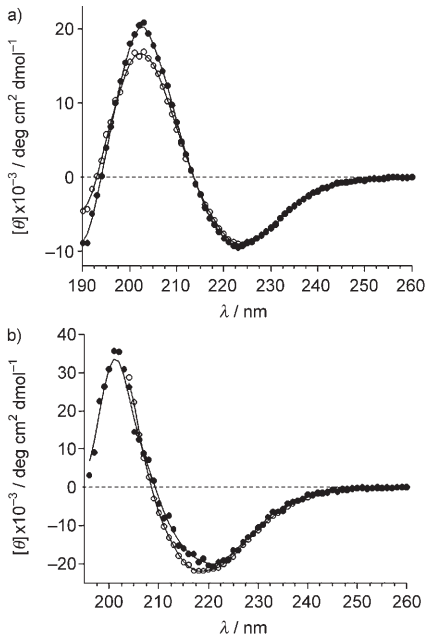

Figure 12. CD spectra of hIAPP17–29 recorded in SUVs of a) DPPC at $T=25\,°C$ (●) and $T=45\,°C$ (○) and b) DPPC/DPPS 3:1 at $T=25\,°C$ (●) and $T=65\,°C$ (○). The experimental conditions chosen to obtain an optimal signal to noise ratio are: peptide concentration $=2\times10^{-5}$ mol dm^{-3}, pH 7.01, lipid/peptide molar ratio 10:1.

Discussion

As anticipated, the present work intended to establish whether the hIAPP17–29 fragment can reproduce some of the key properties of the full-length protein, in terms of conformational behaviour and membrane interaction. To this end, the conformational properties of two short peptide fragments encompassing residues 17–29 of human or rat IAPP were investigated by means of CD and NMR spectroscopy. The 17–29 region is important because it possesses: 1) the minimum amyloidogenic sequence 23–27 (NFGAIL) found in the human sequence, 2) positions 28–29 in which two prolines of the rat sequence replace two serines in the human one; 3) position 18 at which arginine in the rat sequence is replaced by a histidine in the human sequence. The conformational features of these IAPP fragments were explored in water and in different membrane-mimicking environments. The results on the whole confirm that hIAPP17–29 exhibits a conformational polymorphism that depends on the environment, in contrast to rIAPP17–29 that is unstructured in all the experimental conditions employed. hIAPP17–29 shows an extensive β-sheet conformation with a remarkable tendency to self aggregate in aqueous and in diluted SDS solutions, whereas it partially assumes an α-helical conformation in 50% TFE and in an environment (SDS micelles) that mimics the surface of negatively charged membranes. Such a conformational behaviour strongly resembles that exhibited by the full-length IAPP under similar experimental conditions.[66] Furthermore, our conformational studies are in good accord with previously reported secondary-structure predictions that indicated a remarkable tendency of the full-length hIAPP to form β strands in the 25–29 amino acid region.[67,68] However, the majority of predictions for rIAPP show no evidence of substantial secondary structure in the 17–29 region in which all of the amino-acid substitutions occur.[69] In this regard, our CD studies carried out on R18HrIAPP17–29 also show that the replacement of an Arg with a His residue in position 18 does not induce any β-sheet and/or self-association propensity in the rat sequence.

Concerning the NMR study, Mascioni et al. investigated a closely related peptide (hIAPP20–29) and reported that, due to the interaction with negatively charged SDS micelles, the dominant conformation of this peptide is a distorted type I β turn centred on the Phe and Gly residues with Phe, Ala and Ile forming a small hydrophobic cluster that is oriented toward the hydrocarbon region of the micelles with both N and C termini exposed to the solvent.[70] These different conclusions may result from a series of factors. First, a peptide fragment with uncapped N and C termini was used in the above-mentioned study; consequently, the presence of additional charges at both termini might affect the peptide binding to the negatively charged SDS micelles. Moreover, the lack of both N- and C-terminal charges and the presence of the histidine residue in our model might cause a different folding of the peptide chain in the presence of SDS micelles. Unfortunately, Mascioni et al. did not

report a parallel CD study performed in the presence of SDS. The presence of the His residue generates a pH-dependent tendency of hIAPP17–29 to self aggregate, as evidenced by CD and thioflavin-T fluorescence results. In addition, in this case the hIAPP17–29 behaves similarly to the parent full-length protein. In fact, the ionisation state of His18 significantly affects the rate of assembly and the morphology of the aggregates formed by full-length hIAPP, as previously demonstrated by other studies.[33] In particular, the slower rate of fibrillogenesis observed when the His residue is protonated correlates well with the higher solubility of hIAPP at low pH and is ascribed to increased charge–charge repulsions that should also hamper initial oligomerisation. This pH-sensitive conformational polymorphism of hIAPP may have relevant consequences in a biological context. Mature hIAPP is normally stored in the β-cell granules of the pancreas at a pH of 5.5 and is released into the cytoplasmic compartment that has a pH of 7.4. The lower pH of the granule is believed to reduce irreversible aggregation of hIAPP. However, other factors might be involved in controlling amyloidogenesis because hIAPP does not form amyloid in non-diabetic individuals. In this context, it is likely that His18 plays a role in the aggregation of the peptide, but its effect might be masked depending on orientation and depth of penetration of hIAPP in the interior of the membrane.

The DSC analysis of the different lipid/model membrane systems provides an indication concerning the role played by the single residues in the interaction with the membrane. In particular, we have demonstrated the high potential of hIAPP17–29 to interact and perturb DPPC model membranes; based on the negligible interaction of the rat derivative with DPPC, the different membrane activity may result from both the presence of the hydrophobic residue (Phe) in the human sequence and the geometrical hindrance caused by the two prolines in the rat peptide. The titrations of DPPC/hIAPP17–29 systems with copper(II) show that His18 is normally not available to the solvent and the peptide is deeply embedded into the membrane. On the contrary, a control experiment demonstrated that the peptide R18HrIAPP17–29 interacts with DPPC membranes mainly at the water–bilayer interface, thus allowing His to interact with copper(II). Finally, we observed a negligible interaction of hIAPP17–29 with negatively charged DPPC/DPPS membranes. This finding is in contrast to a previous study that suggested that membranes containing phosphatidyl-serine (PS) lipids may promote α helix→β sheet conversion as well as aggregation in full-length hIAPP.[52] According to that paper, the increased local concentration of the peptide at the negatively charged membrane surface, coupled with the anisotropic properties of the membrane, would facilitate the interaction of membrane-bound peptides leading to the formation of oligomeric membrane-active β-sheet aggregates. Perhaps our different conclusions result from the poor solubility of hIAPP17—29, due to its high propensity to self assemble into amyloid-like structures. It is likely that the presence of negatively charged DPPS membrane surfaces even enhances the aggregation rate of this fragment, which promptly self assembles into large aggregates, ruling out any chance to form smaller oligomeric membrane-active structures. This is in accordance with the current view that mature fibrils are inert.

In conclusion, we provide evidence that small model peptides encompassing residues 17–29 are able to reproduce both the membrane affinity and the conformational behaviour of the full-length IAPP and demonstrate the role played by single residues in determining their properties.

Experimental Section

Materials: Peptide-coupling reagents and peptide-synthesis resins were purchased from Applied Biosystems. Amino acids were purchased form NovaBiochem. 1,2-Dipalmitoyl-*sn*-glycero-3-phosphocholine (DPPC) and 1,2-dipalmitoyl-*sn*-glycero-3-phosphoserine (DPPS) were obtained from Fluka. All inorganic salts for phosphate-buffer preparation were purchased from SIGMA. All protected amino-acid derivatives were obtained from Novabiochem (Switzerland). All other chemicals were of the highest-available grade and were used without further purification.

Solid-phase peptide synthesis: The 9-fluorenylmethyloxycarbonyl (Fmoc)-amino-acid side-chain protection was selected as follows: *tert*-butyl, *t*But (Ser); trityl, Trt (Asn, His); Pbf (Arg). Generally, the peptide chains were assembled on a polyethylene glycol–polystyrene resin (PAL-PEG-PS) (with a substitution level of 0.22 mequiv g^{-1}) by using an Applied Biosystems Pioneer peptide synthesiser. All residues were introduced according to the HATU/DIEA activation method. A four-fold amino-acid excess was used for each coupling cycle. N-terminal acetylation of peptide chains was performed by treating the fully assembled and protected peptide resins (after removal of the N-terminal Fmoc group) with a solution containing acetic anhydride (6% v/v) and DIEA (5% v/v) in DMF. A mixture of trifluoroacetic acid (TFA)/H_2O/triisopropylsilane (TIS) (95:2.5:2.5 v/v/v) was used for the deprotection and resin cleavage of the peptides. The crude peptides were precipitated with cold diethyl ether and then lyophilised. Purification of the peptides was carried out by preparative RP-HPLC using a Vydac C-18 column (250× 22 mm, 300 Å pore size, 10–15 μm particles) with a linear gradient of acetonitrile/water containing 0.1% TFA (from 15 to 40% acetonitrile, flow rate 10 mL min^{-1}). The identity and purity of the peptides were confirmed by electrospray ionisation mass spectrometry (ESI-MS) and analytical RP-HPLC, respectively. ESI-MS: hIAPP17—29: *m*/*z*: calcd for $C_{59}H_{92}N_{18}O_{20}$ $[M+H]^+$: 1372.67; found: 1373.5; rIAPP17—29: *m*/*z*: calcd for $C_{61}H_{103}N_{19}O_{18}$ $[M+H]^+$: 1389.77; found: 1390.5; R18HrIAPP17—29: *m*/*z*: calcd for $C_{61}H_{98}N_{18}O_{18}$ $[M+H]^+$: 1371.36; found: 1372.20.

Circular dichroism (CD) spectra: The CD spectra were obtained at 300 K under a constant flow of N_2 by using a Jasco J-810 spectropolarimeter that had been calibrated with an aqueous solution of (1*R*)-(−)-10-camphorsulfonic acid, ammonium salt.[71] Experimental measurements were conducted under varying experimental conditions, such as different pH, different percentages of aqueous TFE, SDS concentrations and lipid membranes. The CD spectra were recorded in the UV region (190–260 nm) by using a 1-mm-pathlength cuvette with peptide concentrations of 1.0×10^{-5} mol dm^{-3}. The spectra represent the average of 8–20 scans. CD intensities are expressed as mean residue ellipticity $[\theta]$ (deg cm^2 $dmol^{-1}$).

Thioflavin-T-assay: Fluorescence was monitored as a function of time in a 1.0-cm-pathlength quartz cuvette by using a Spex Fluorolog-2 (mod. F-111) spectrofluorimeter. Two identical stock solutions of the hIAPP17–29 or rIAPP17–29 were prepared by dissolving 5 mg per mL of the peptide fragments in 100% hexafluoroisopropanol (HFIP). Experiments were performed by diluting 25 μL of peptide stock into 2.25 mL of 5×10^{-2} mol dm^{-3} citrate/phosphate buffer, pH 7.40 or pH 4.00 containing thioflavine-T (ThT). Final solutions were 3.76×10^{-5} mol dm^{-3} ThT and contained 3.6×10^{-5} mol dm^{-3} (0.002 mg per mL) peptide in 1% HFIP. All buffer solutions were filtered by using a 0.2 μm filter. The measure-

ments were carried out by using, as a control, the time dependence of the fluorescence of thioflavine-T solutions without the peptide at both pH values. The sample mixtures were monitored over a 30-min period at an excitation wavelength of 442 nm and the emission was 485 nm. Both excitation and emission bandwidths were set to 2 nm.[72,73]

NMR spectroscopy: All NMR spectra were acquired at 27 °C by using a Varian INOVA Unity-plus spectrometer operating at 499.884 MHz. Lyophilised samples of 1×10^{-3} mol dm^{-3} concentration were dissolved in 1.7×10^{-1} mol dm^{-3} SDS_{-d25} in 90:10 H_2O/D_2O (hIAPP17–29) or 90:10 H_2O/D_2O (rIAPP17–29). Trimethylsilylpropionic acid (TSP) was used as an internal standard. The pH of the solution was adjusted to pH 5.5 by adding the appropriate acid or base solution. The electrode-measured pH value was uncorrected for the isotope effect. 1D spectra were generally acquired with 32K data points over a spectral width of 6000 Hz. 2D experiments were typically acquired with 2048 data points in the t_2 dimension and 512 t_1 increments. Water saturation was achieved by low-power irradiation during the relaxation delay. TOCSY spectra were acquired with a spin locking field of 7 kHz at a mixing time of 80 ms. ROESY spectra were run by using a 2-kHz spin-locking field at a mixing time of 300 ms. Mixing times of 150 and 250 ms were used in the NOESY experiments.

Preparation of model membranes: Model membranes were prepared as described elsewhere.[61] Briefly, solutions of pure phospholipids in $CHCl_3$ were dried under a nitrogen flow and evaporated under high vacuum to dryness in round-bottomed flasks. The resulting lipid film on the wall of the flask was hydrated with an appropriate volume of 1×10^{-5} mol dm^{-3} phosphate buffer and dispersed by vigorous stirring in a water bath set at 4 °C above the transition gel—liquid–crystals temperature of the membrane. The final concentration of the lipid was 2 mg mL^{-1}. To obtain large unilamellar vesicles (LUVs), the multilamellar vesicles (MLVs) so obtained were extruded through polycarbonate filters (pore size = 100 nm) (Nuclepore, Pleasanton, CA) mounted in a mini-extruder (Avestin Inc.) fitted with two 0.5-mL Hamilton gastight syringes (Hamilton, Reno, NV). Usually, we subjected samples to 19 passes through two filters in tandem. Small unilamellar vesicles (SUV) were prepared by sonication of MLVs and were used for CD experiments in order to decrease scattering phenomena. Typically, 1-mL volumes were sonicated for 45 min above the respective transition temperatures (T_m) of the phospholipids with a 90% duty cycle. Sonicated vesicles were rapidly cooled to RT and were used within 45 min to prevent coalescence.

Incorporation of peptide fragments in model membranes: Two different protocols were applied to prepare mixed lipid/peptide bilayers: A) the peptide fragment was initially dissolved in the same organic solution ($CHCl_3$) of the phospholipid and subsequently, the lipid film was hydrated and extruded/sonicated according to the above-described procedure; B) a proper amount of peptide was added to previously prepared DPPC or 3:1 DPPC/DPPS (LUVs or SUVs) suspensions, vortexed for 15 min and immediately analysed. The peptide/lipid ratio was kept fixed at 1:10 in all the experiments. The full-length human and rat IAPP peptides (hIAPP and rIAPP) were incorporated into DPPC model membranes according to method A; the molar ratio peptide/lipid was decreased down to 1:50 because of the higher molecular weight of the entire IAPP peptides.

Differential scanning calorimetry: DSC scans were carried out by using a second-generation high-sensitivity SETARAM micro differential scanning calorimeter (microDSC II) with 1-mL stainless-steel sample cells, interfaced with a BULL 200 Micral computer. The sampling rate was one point/second in all measuring ranges. The buffer solution without the sample was used in the reference cell. Both the sample and reference were heated with a precision of 0.05 °C at a scanning rate of 0.5 °C min^{-1}. To obtain the excess heat capacity ($c_{p(exc)}$) curves, buffer–buffer baselines were recorded at the same scanning rate and then subtracted from the sample curve. Calibration in energy was obtained by giving a definite power supply, electrically generated by an EJ2 SETARAM Joule calibrator within the sample cell. To check the reproducibility of the results, three different samples were analysed. All DSC experiments were repeated after 24 and 48 h, but kinetic effects were never evidenced.

Acknowledgements

This work was supported by the European Project EURAMY (contract no. 037525) and MiUR Grants 196 D.M. 1105/2002, PRIN 2005035582, FIRB RBNE03PX83, FIRB RBN04L28Y. CNR is also acknowledged for partial financial support.

[1] J. B. Martin, *N. Engl. J. Med.* **1999**, *340*, 1970–1980.
[2] M. Stefani, C. M. Dobson, *J. Mol. Med.* **2003**, *81*, 678–699.
[3] G. Merlini, V. Bellotti, *N. Engl. J. Med.* **2003**, *349*, 583–596.
[4] J. D. Sipe, *Crit. Rev. Clin. Lab. Sci.* **1994**, *31*, 325–354.
[5] J. P. Taylor, J. Hardy, K. H. Fischbeck, *Science* **2002**, *296*, 1991–1995.
[6] D. L. Price, P. C. Wong, A. L. Markowska, M. K. Lee, G. Thinakaren, D. W. Cleveland, S. S. Sisodia, D. R. Borchelt, *Ann. N. Y. Acad. Sci.* **2000**, *920*, 179–191.
[7] C. D. Link, *Mech. Ageing Dev.* **2001**, *122*, 1639–1649.
[8] S. B. Prusiner, *Proc. Natl. Acad. Sci. USA* **1998**, *95*, 13363–13383.
[9] V. N. Uversky, *Cell. Mol. Life Sci.* **2003**, *60*, 1852–1871.
[10] G. G. Glenner, C. W. Wong, *Biochem. Biophys. Res. Commun.* **1984**, *120*, 885–890.
[11] C. L. Masters, G. Simms, N. A. Weinman, G. Multhaup, B. L. McDonald, K. Beyreuther, *Proc. Natl. Acad. Sci. USA*, **1985**, *82*, 4245–4249.
[12] B. Ahren, C. Oosterwijk, C. J. Lips, J. W. Hoppener, *Diabetologia*, **1998**, *41*, 1374–1380.
[13] P. Westermark, E. Wilander, D. W. Hayden, T. D. O'Brian, K. H. Johnson, *Proc. Natl. Acad. Sci. USA* **1987**, *84*, 3881.
[14] S. E. Kahn, S. Andrikopoulos, C. B. Verchere, *Diabetes* **1999**, *48*, 241–246.
[15] E. Jaikaran, A. Clark, *Biochim. Biophys. Acta*, **2001**, *1537*, 179–203.
[16] A. Kapurniotu, *Biopolymers* **2001**, *60*, 438–459.
[17] C. F. Howard, Jr., *Diabetes* **1978**, *27*, 357–364.
[18] B. L. Yano, D. W. Hayden, K. H. Johnson, *Vet. Pathol.* **1981**, *18*, 621–627.
[19] C. Betsholtz, L. Christmanson, U. Engstrom, F. Rorsman, V. Svensson, K. H. Johnson, P. Westermark, *FEBS Lett.* **1989**, *251*, 261–265.
[20] K. H. Johnson, T. D. O'Brien, C. Betsholtz, P. Westermark, *Lab. Invest.* **1992**, *66*, 522–535.
[21] A. Lorenzo, B. Razzaboni, G. C. Weir, B. A. Yankner, *Nature* **1994**, *368*, 756–760.
[22] P. Westermark, U. Engstrom, K. H. Johnson, G. Westermark, C. Betsholtz, *Proc. Natl. Acad. Sci. Usa*, **1990**, *87*, 5036–5040.
[23] T. T. Ashburn, M. Auger, P. T. Lansbury, *J. Am. Chem. Soc.* **1992**, *114*, 790–791.
[24] T. T. Ashburn, P. T. Lansbury, *J. Am. Chem. Soc.* **1993**, *115*, 11012–11013.
[25] D. F. Moriarty, D. P. Raleigh, *Biochemistry* **1999**, *38*, 1811–1818.
[26] M. R. Nilsson, D. P. Raleigh, *J. Mol. Biol.* **1999**, *294*, 1375–1385.
[27] E. T. Jaikaran, C. E. Higham, L. C. Serpell, J. Zurdo, M. Gross, A. Clark, P. E. Fraser, *J. Mol. Biol.* **2001**, *308*, 515–525.
[28] C. Goldsbury, K. Goldie, J. Pellaud, J. Seeling, P. Frey, S. A. Muller, J. Kistler, G. J. S. Cooper, U. Aebi, *J. Struct. Biol.* **2000**, *130*, 352–362.
[29] K. Tenidis, M. Waldner, J. Bernhagen, W. Fischle, M. Bergmann, M. Weber, M. L. Merkle, M. L. Voelter, H. Brunner, A. Kapurniotu, *J. Mol. Biol.* **2000**, *295*, 1055–1071.
[30] D. Zanuy, B. Ma, R. Nussinov, *Biophys. J.* **2003** *84*, 1884–1894.
[31] J. Green, C. Goldsbury, T. Mini, S. Sunderji, P. Frey, J. Kistler, G. Cooper, U. Aebi, *J. Mol. Biol.* **2003**, *326*, 1147–1156.
[32] L. A. Scrocchi, K. Ha, Y. Chen, L. Wu, F. Wang, P. E. Fraser, *J. Struct. Biol.* **2003**, *141*, 218–227.
[33] A. Abedini, D. P. Raleigh, *Biochemistry* **2005**, *44*, 16284–16291.
[34] A. V. Kajava, U. Aebi, A. C. Steven, *J. Mol. Biol.* **2005**, *348*, 247–252.
[35] E. T. A. S. Jaikaran, C. E. Higham, L. C. Serpell, J. Zurdo, M. Gross, A. Clark, P. E. Fraser, *J. Mol. Biol.* **2001**, *308*, 515–525.
[36] M-C. Lin, T. Mirzabekov, B. L. Kagan, *J. Biol. Chem.* **1997**, *272*, 44–47.

[37] Y. Hirakura, B. L. Kagan, *J. Neurosci. Res.* **1999**, *57*, 458–466.
[38] Y. Hirakura, B. L. Kagan, *Amyloid* **2001**, *8*, 94–100.
[39] N. Arispe, H. B. Pollard, E. Rojas, *Proc. Natl. Acad. Sci. USA* **1993**, *90*, 10573–10577.
[40] K. Matsuzaki, C. Horikiri, *Biochemistry* **1999**, *38*, 4137–4142.
[41] J. J. Kremer, M. M. Pallitto, D. J. Sklansky, R. Murphy, *Biochemistry* **2000**, *39*, 10309–10318.
[42] M. J. Volles, S. J. Lee, J. C. Rochet, M. D. Shtilerman, T. T. Ding, J. C. Kessler, P. T. Lansbury, Jr., *Biochemistry* **2001**, *40*, 7812–7819.
[43] J. Kazlauskaite, N. Sanghera, I. Sylvester, C. Venien-Bryan, T. J. Pinheiro, *Biochemistry* **2003**, *42*, 3295–3304.
[44] M. Bokvist, F. Lindstrom, A. Watts, G. Grobner, *J. Mol. Biol.* **2004**, *335*, 1039–1049.
[45] A. Quist, I. Doudevski, H. Lin, R. Azimova, D. Ng, B. Frangione, B. Kagan, J. Ghiso, R. Lal, *Proc. Natl. Acad. Sci. USA* **2005**, *102*, 10427–10432.
[46] C. M. Dobson, *Nature* **2003**, *426*, 884–890.
[47] T. A. Mirzabekov, M. C. Lin, B. L. Kagan, *J. Biol. Chem.* **1996**, *271*, 1988–1992.
[48] B. Kurganov, M. Doh, N. Arispe, *Peptides*, **2004**, *25*, 217–232.
[49] M. Anguiano, R. J. Nowak, P. T. Lansbury, Jr., *Biochemistry* **2002**, *41*, 11338–11343.
[50] B. L. Kagan, R. Azimov, R. Azimova, *J. Membr. Biol.* **2004**, *201*, 1–10.
[51] J. D. Knight, A. D. Miranker, *J. Mol. Biol.* **2004**, *341*, 1175–1187.
[52] S. A. Jayasinghe, R. Langen, *Biochemistry* **2005**, *44*, 12113–12119.
[53] A. Perczel, M. Hallosi in *Circular Dichroism and the Conformational Analysis of Biomolecules* (Ed.: G. D. Fasman), Plenum Press, New York, **1996**, pp. 285–380.
[54] M. R. Kallenbach, P. Lyn, H. Zhou in *Circular Dichroism and the Conformational Analysis of Biomolecules*, (Ed.: G. D. Fasman), Plenum Press, New York, **1996**, pp. 201–259.
[55] R. Monserret, M. J. McLeish, A. Beckmann, C. Geonzjann, F. Penin, *Biochemistry* **2000**, *39*, 8362–8373.
[56] a) R. C. Hund, *J. Magn. Reson.* **1989**, *87*, 422–428; b) M. van Kienlin, C. T. W. Moonen, A. van der Toorn, P. C. Van Zijl, *J. Magn. Reson.* **1991**, *93*, 423–429.
[57] A. Bax, D. G. Davis, *J. Magn. Reson.* **1985**, *65*, 355–360.
[58] J. Jeener, B. H. Meier, P. Beckmann, R. R. Ernst, *J. Chem. Phys.* **1979**, *71*, 4546–4553.
[59] K. Wuthrich, *NMR of Proteins and Nucleic Acids*, Wiley Interscience, New York, **1986**.
[60] D. S. Wishart, C. G. Bigam, A. Holm, R. S. Hodges, B. D. Sykes, *J. Biomol. NMR* **1995**, *5*, 67–81.
[61] D. Grasso, D. Milardi, C. La Rosa, E. Rizzarelli, *New J. Chem.* **2001**, *25*, 1543–1548.
[62] R. C. MacDonald R. I. MacDonald, B. P. Menco, K. Takeshita, N. K. Subarrao, L. R. Hu, *Biochim. Biophys. Acta* **1991**, *1061*, 297–303.
[63] J. M. Sanderson, *Org. Biomol. Chem.* **2005**, *3*, 201–212.
[64] J. F. Nagle, *Annu. Rev. Phys. Chem.* **1980**, *31*, 175–195.
[65] D. Chapman in *Biological Membranes*, Academic Press, New York, **1982**, Vol. 4, p. 179.
[66] J. D. Knight, J. A. Hebda, A. D. Miranker, *Biochemistry* **2006**, *45*, 9496–9508.
[67] C. Wu, H. Lei, Y. Duan, *Biophys. J.* **2004**, *87*, 3000–3009.
[68] C. Wu, H. Lei, Y. Duan, *Biophys. J.* **2005**, *88*, 2897–2906.
[69] J. Green, C. Goldsbury, T. Mini, S. Sunderji, P. Frey, J. Kistler, G. Cooper, U. Aebi, *J. Mol. Biol.* **2003**, *326*, 1147–1156.
[70] A. Mascioni, F. Porcelli, U. Ilangovan, A. Ramamoorthy, G. Veglia, *Biopolymers* **2003**, *69*, 29–41.
[71] G. C. Chen, J. T. Yang, *Anal. Lett.* **1977**, *10*, 1195–1207.
[72] H. Naiki, K. Higuchi, M. Hosokawa, T. Takeda, *Anal. Biochem.* **1989**, *177*, 244–249.
[73] H. LeVine, *Methods Enzymol.* **1999**, *309*, 274–284.

Received: April 13, 2007
Revised: July 10, 2007
Published online: September 28, 2007

